ARTICLES

Two interacting electrons in a box: An exact diagonalization study

Ali Alavi[a)]
School of Mathematics and Physics, Queen's University, Belfast BT7 1NN, United Kingdom and
Department of Chemistry, University of Cambridge, Lensfield Road, Cambridge CB2 1EW, United Kingdom

(Received 31 May 2000; accepted 17 August 2000)

The behavior of two electrons confined to a three-dimensional box with infinite walls and interacting with a Coulomb potential is studied using an exact diagonalization technique. The use of symmetry operators enables the Hamiltonian to be block diagonalized. Apart from the total spin, the wavefunctions can be classified using three symmetry quantum numbers. The Coulomb integrals are shown to be amenable to efficient and accurate calculation. The energy of the lowest few eigenstates of both the singlet ($S=0$) and triplet ($S=1$) are calculated as a function of the box size (i.e., in effect r_s) for a slightly tetragonally distorted box where the *z*-axis is longer than the *x*- and *y*-axes. The ground state is a singlet function with ggg symmetry at all densities. At small r_s, the ground state has a maximum in electron density at the box center. Upon increasing r_s, at $r_s \approx 8$ a.u., the ground state density acquires a minimum in the box center. At this same r_s, the first-excited state of the singlet manifold changes its symmetry from ggu to ugu, and the corresponding degeneracy is changed from one to two. The energy-r_s curve shows a nonanalytic change in slope. Subsequent increasing of r_s gives rise to increased localization of the charge density in the eight corners of the box, which can be identified as the ''Wigner'' crystal limit of the present model. The physical exchange-correlation hole is evaluated in the high and low density limits. © *2000 American Institute of Physics.* [S0021-9606(00)31542-2]

I. INTRODUCTION

Interest in correlated electron systems, and electron exchange and correlation, is as strong as ever.[1,2] In this paper we study a very simple, possibly the simplest, correlated electronic system with realistic interactions, namely two electrons interacting with a Coulomb potential in a box bounded with infinite walls. The problem is studied in a quasi-exact and nonpertubative way using exact diagonalization.

The model can be motivated in a number of ways. It is a well-defined and physical interacting system in which essentially exact solutions for the ground and excited states can be obtained. The model can be viewed as a quantum-confinement problem, in which the correlation in the system can be increased or decreased simply by varying the box size, going from the dense (weakly correlated) to the dilute (strongly correlated) limit. It is desirable to treat the different regimes on the same footing. In addition, the system is essentially nonuniform (the hard-wall boundary conditions take care of that), and the resulting exact solutions may provide different, and complementary, model systems to study exchange-correlation, as compared to the uniform electron gas. Part of the motivation of this work, reported in a later publication, will be the construction of exact exchange-correlation holes, which could provide new input data for constructing approximate density functionals. As Perdew *et al.*[3] have emphasized, the use of *physical* exchange-correlation holes is essential in constructing such functionals within, say, the generalized gradient approximation. Exactly solvable model systems in which the formalism of density functional theory[4–6] can be implemented provide the very rare opportunity to examine, without uncontrolled approximations, the complex nature of the exchange-correlation hole. The ''Hooke's Law'' helium atom[7–10] is one such extensively studied two-electron model with a central attractive center, in which the electron–nuclear Coulomb attraction is replaced by a harmonic potential. The present system of two electrons confined to a three-dimensional box with no attractive center provides a different sort of physical system in which the correlation is between essentially free electrons. Although the present system is of considerable conceptual interest, applications of related systems to model quantum dots can be envisaged, for example, to investigate the effect of reduced dimensionality (in particular two dimensions), alternative geometries and confining potentials. These will be pursued in later work. Last, but not least, it is worth stating that the behavior of many-electron systems can be extremely complex: studying simple models in which exact solutions can be obtained may be instructive.

The paper is organized as follows. In Sec. II the general method of solution is provided. In Sec. III we discuss the role of symmetries in this problem. In Sec. IV the evaluation of the Coulomb integrals in a basis of trigonometric func-

a)Electronic mail: alavi@theor.ch.cam.ac.uk

tions is discussed in detail. In Sec. V we give details on the calculation of the electron density and exchange-correlation hole. In Sec. VI we report the results of several calculations of this system, including energies and wavefunctions. Section VII is the conclusion. Two technical appendices give an account of a real-space method to evaluate the Coulomb integrals.

II. METHOD OF SOLUTION

It is natural to seek the solutions to the Schrödinger equation for two electrons in a box with infinite potential in terms of trigonometric functions. To this end let $\Psi(\mathbf{x}_1,\mathbf{x}_2)$ be a two-body wavefunction, which can be expressed as a product of a spatial wavefunction $\Psi^{\pm}(\mathbf{r}_1,\mathbf{r}_2)$ and a spin wavefunction $\chi^{\mp}(\sigma_1,\sigma_2)$:

$$\Psi(\mathbf{x}_1,\mathbf{x}_2)=\Psi^{\pm}(\mathbf{r}_1,\mathbf{r}_2)\chi^{\mp}(\sigma_1,\sigma_2). \tag{1}$$

Two types of solutions are present: singlet spin ($\chi^-, S=0$) and triplet spin ($\chi^+, S=1$), corresponding, respectively, to symmetric (Ψ^+) and anti-symmetric (Ψ^-) spatial functions. We will expand the spatial wavefunction in terms of linear combinations of symmetrized (or anti-symmetrized) sine functions $\Phi^{\pm}_{nmlpqr}(\mathbf{r}_1,\mathbf{r}_2)$:

$$\Phi^{\pm}_{nmlpqr}(\mathbf{r}_1,\mathbf{r}_2)=N_{nmlpqr}\{u_{nml}(\mathbf{r}_1)u_{pqr}(\mathbf{r}_2) \pm u_{pqr}(\mathbf{r}_1)u_{nml}(\mathbf{r}_2)\}, \tag{2}$$

with

$$u_{nml}(\mathbf{r})=\sqrt{\frac{8}{\Omega}}\sin(n\pi x/L_x)\sin(m\pi y/L_y)\sin(l\pi z/L_z), \tag{3}$$

where L_x, L_y and L_z are the box dimensions and $\Omega = L_xL_yL_z$ is the volume. In (2), N_{nmlpqr} is chosen so as to normalize the function, i.e.,

$$N_{nmlpqr}=\frac{1}{\sqrt{2+2.\delta_{np}\delta_{mq}\delta_{lr}}}. \tag{4}$$

In addition, the antisymmetric function $\Phi^{-}_{nmlnml}(\mathbf{r}_1,\mathbf{r}_2)$ identically vanishes. If we denote

$$\mathbf{G}=\pi\left(\frac{n}{L_x},\frac{m}{L_y},\frac{l}{L_z},\frac{p}{L_x},\frac{q}{L_y},\frac{r}{L_z}\right), \tag{5}$$

then $\Psi^{\pm}(\mathbf{r}_1,\mathbf{r}_2)$ can be expressed as:

$$\Psi^{\pm}(\mathbf{r}_1,\mathbf{r}_2)=\sum_{\mathbf{G}} c^{\pm}_{\mathbf{G}}\Phi^{\pm}_{\mathbf{G}}(\mathbf{r}_1,\mathbf{r}_2), \tag{6}$$

where $c^{\pm}_{\mathbf{G}}$ are real linear coefficients to be determined, and the sum over $\mathbf{G}$ runs over the set of all positive integers $\{n,m,l,p,q,r\}$. $\Phi^{\pm}_{\mathbf{G}}(\mathbf{r}_1,\mathbf{r}_2)$ form a complete symmetric (or anti-symmetric) set of basis functions which satisfy the boundary conditions that the wavefunctions vanish at the boundaries. Therefore, any symmetric (or anti-symmetric) satisfying the same boundary conditions can be expressed using them.

The two-electron Hamiltonian (in Hartree atomic units $\hbar=m_e=e^2=1$) for the problem at hand is

$$\hat{H}=\hat{T}+\hat{U}+\hat{V}, \tag{7}$$

$$\hat{T}=-\frac{1}{2}\sum_{i=1}^{2}\nabla_i^2, \tag{8}$$

$$\hat{U}=\frac{1}{|\mathbf{r}_1-\mathbf{r}_2|}, \tag{9}$$

$$\hat{V}=\sum_i v(\mathbf{r}_i), \tag{10}$$

where

$$v(x,y,z)=\begin{cases}0, & \text{for } 0<x<L_x,\quad 0<y<L_y,\quad 0<z<L_z,\\ \infty, & \text{otherwise.}\end{cases} \tag{11}$$

In the chosen basis, the kinetic energy is diagonal:

$$\langle\mathbf{G}|\hat{T}|\mathbf{G}'\rangle=\frac{\pi^2}{2}\left(\frac{n^2+p^2}{L_x^2}+\frac{m^2+q^2}{L_y^2}+\frac{l^2+r^2}{L_z^2}\right)\delta_{\mathbf{GG}'}. \tag{12}$$

The matrix elements of the Coulomb operator in the basis of sine functions, $\langle\mathbf{G}|\hat{U}|\mathbf{G}'\rangle$, requires extensive consideration, and is dealt with in Sec. IV; For the present we assume that the Coulomb matrix elements can be calculated accurately and efficiently.

We seek solutions to the Schrödinger equation,

$$H\Psi^{\pm}=E^{\pm}\Psi^{\pm}, \tag{13}$$

as an eigenvalue equation in the $c^{\pm}_{\mathbf{G}}$:

$$\sum_{\mathbf{G}'} H_{\mathbf{GG}'}c^{\pm}_{\mathbf{G}'}=E^{\pm}c^{\pm}_{\mathbf{G}}. \tag{14}$$

The procedure is so far exact, and if carried out, the resulting wavefunctions $\Psi^{\pm}$ would be the exact solutions to the problem, including the excited states. It is a matter as to how many basis functions $\Phi^{\pm}_{\mathbf{G}}$ can be included in practice.

Let $n_{\max}$ denote the highest wavenumber to be allowed in the basis of u's [Eq. (3)]. If we neglect the use of any additional symmetries, the total number of basis functions $N^{\pm}_{\text{basis}}$ for symmetric and anti-symmetric solutions is

$$N^{\pm}_{\text{basis}}=\frac{{n_{\max}}^3.({n_{\max}}^3\pm 1)}{2}. \tag{15}$$

Evidently, this is a rapidly growing number with $n_{\max}$. For example, $n_{\max}=5$ gives $N_{\text{basis}}\sim 7800$, and $n_{\max}=10$ gives $N_{\text{basis}}\sim 500000$. In order to make the problem more manageable we can appeal to symmetries inherent in the two-electron Hamiltonian.

III. SYMMETRY

A significant reduction in basis set size, and therefore computational effort, can be achieved by recognizing the role of symmetry in the present model. In general for a cuboidal box (with $L_x\neq L_y\neq L_z$), there are three symmetry operators which leave the Hamiltonian (7) invariant, namely reflection operations in the xy, xz and yz planes, respectively. These correspond to the transformations

$$x \to L_x - x, \tag{16}$$

$$y \to L_y - y, \tag{17}$$

$$z \to L_z - z, \tag{18}$$

being applied to the components of all the electrons simultaneously. Let us denote the corresponding operators $\hat{P}_x, \hat{P}_y, \hat{P}_z$, i.e.,

$$\hat{P}_x \Psi(x_1, y_1, z_1, x_2, y_2, z_2) = \Psi(L_x - x_1, y_1, z_1, L_x - x_2, y_2, z_2), \tag{19}$$

with similar definitions for $\hat{P}_y$ and $\hat{P}_z$. It is easily verified that the symmetry operators each commute with the Hamiltonian, and with each other. Therefore, the eigenstates of the Hamiltonian can be labeled according to the quantum numbers of the symmetry operators, which are $+1$ for even functions (*gerade*) and -1 for odd functions (*ungerade*). The basis functions can be classified accordingly:

$$\hat{P}_x \Phi_{nmlpqr} = (-1)^{n+p} \Phi_{nmlpqr}, \tag{20}$$

$$\hat{P}_y \Phi_{nmlpqr} = (-1)^{m+q} \Phi_{nmlpqr}, \tag{21}$$

$$\hat{P}_z \Phi_{nmlpqr} = (-1)^{l+r} \Phi_{nmlpqr}. \tag{22}$$

The overall wavefunction Ψ can be labeled according to these three quantum numbers. Thus in general we will have eight manifolds:

$$\Psi_{ggg}, \Psi_{ugg}, \Psi_{gug}, \Psi_{uug}, \Psi_{ggu}, \Psi_{ugu}, \Psi_{guu}, \Psi_{uuu},$$

and each manifold will contain nonzero components of the basis functions Φ_{nmlpqr} with the same symmetry. Therefore, the Hamiltonian block diagonalizes into eight smaller problems, each of which is approximately one-eighth of the size of the Hamiltonian expressed in the full basis. For example, the ggg manifold will mix states such as $|111111\rangle$, $|111113\rangle$, $|111131\rangle, \ldots$, etc., all of which have ggg symmetry, but not $|111112\rangle$, $|111121\rangle, \ldots$, etc. which have ggu symmetry.

Additional symmetries may also exist for special geometries of the box. For example, for a cubic box, i.e., $L_x = L_y = L_z$, there are additional reflection and rotational symmetries. In these cases a further reduction in basis set size can be achieved through the use of appropriately symmetrized combinations of the basis functions. In such cases, some of the manifolds will be degenerate. For example, for a cube, the ggu gug and ugg manifolds are degenerate.

IV. COULOMB INTEGRALS

In order to calculate the matrix elements of the Hamiltonian, we need to evaluate the following types of integrals:

$$(nmlpqr|n'm'l'p'q'r') \equiv \int \cdots \int \frac{u^*_{nml}(\mathbf{r}_1) u^*_{pqr}(\mathbf{r}_2) u_{n'm'l'}(\mathbf{r}_1) u_{p'q'r'}(\mathbf{r}_2)}{|\mathbf{r}_1 - \mathbf{r}_2|} \times d\mathbf{r}_1\, d\mathbf{r}_2, \tag{23}$$

where $u_{nml}(\mathbf{r})$ is given by Eq. (3). The limits of the integration run from $\{x_1, x_2 : 0, L_x\}$, $\{y_1, y_2 : 0, L_y\}$ and $\{z_1, z_2 : 0, L_z\}$. The Coulomb integrals between the symmetrized or antisymmetrized basis functions are given by the sum and difference, respectively, of the direct $(nmlpqr|n'm'l'p'q'r')$ and exchange $(nmlpqr|p'q'r'n'm'l')$ integrals:

$$\langle \Phi^{\pm}_{\mathbf{G}} | \hat{U} | \Phi^{\pm}_{\mathbf{G}'} \rangle = 2\{(nmlpqr|n'm'l'p'q'r') \pm (nmlpqr|p'q'r'n'm'l')\} \times N_{nmlpqr} N_{n'm'l'p'q'r'}. \tag{24}$$

It is convenient first of all to transform to scaled units:

$$x'_1 = x_1 / L_x, \quad y'_1 = y_1 / L_y, \quad z'_1 = z_1 / L_z, \tag{25}$$

and similarly for x_2, y_2 and z_2. In what follows, in order to keep the notation as uncluttered as possible, we shall refer to x'_1 as x_1. Defining the ratio of the box vectors as

$$b = L_y / L_x, \quad c = L_z / L_x, \tag{26}$$

we can express the integrals as

$$\frac{2^6}{L_x} \int_0^1 \cdots \int_0^1 \sin(n\pi x_1) \sin(m\pi y_1) \sin(l\pi z_1) \sin(p\pi x_2) \sin(q\pi y_2) \sin(r\pi z_2) \times \frac{\sin(n'\pi x_1) \sin(m'\pi y_1) \sin(l'\pi z_1) \sin(p'\pi x_2) \sin(q'\pi y_2) \sin(r'\pi z_2)}{|\mathbf{r}_1 - \mathbf{r}_2|} d\mathbf{r}_1\, d\mathbf{r}_2, \tag{27}$$

where

$$|\mathbf{r}_1 - \mathbf{r}_2| = \sqrt{(x_1 - x_2)^2 + b^2 (y_1 - y_2)^2 + c^2 (z_1 - z_2)^2}. \tag{28}$$

We tried two methods of evaluating this integral: (i) by transformation to center-of-mass and relative coordinates (ii) a Fourier-space method. The second method turned out to be more convenient, and will be outlined in detail below. Details of the first method are given in Appendices A & B.

In the Fourier method, we first write $1/|\mathbf{r}_1 - \mathbf{r}_2|$ as a Fourier sum over the wave-vectors of the box:

$$\frac{1}{|\mathbf{r}_1 - \mathbf{r}_2|} = \sum_{\mathbf{g}} v_{\mathbf{g}} e^{i\mathbf{g}\cdot(\mathbf{r}_1 - \mathbf{r}_2)}, \tag{29}$$

with

$$v_{\mathbf{g}} = \frac{1}{\Omega'} \int_{\Omega'} \frac{e^{-i\mathbf{g}.\mathbf{r}}}{|\mathbf{r}|} d\mathbf{r}, \tag{30}$$

where the region of integration Ω' runs overs the maximum possible relative displacements of the two particles in scaled

units, i.e., $\{x:-1,1\}$, $\{y:-1,1\}$ and $\{z:-1,1\}$. Therefore, $\Omega'=8ab$. The wave-vectors which enter the Fourier sum have the form

$$\mathbf{g}=\pi(g_x,g_y,g_z), \tag{31}$$

where g_x,g_y,g_z runs over all integers (positive and negative). Note that, because of the cuboidal boundary conditions, the form for $v_{\mathbf{g}}$ is not precisely $4\pi/g^2$, and is in fact anisotropic. The method by which the Fourier integral is calculated is discussed later on. Note also that the vector $\mathbf{g}$ is unrelated to the vector $\mathbf{G}$ which label the basis functions.

Upon substitution of the Fourier sum (29) into the Coulomb integral (23), and noting that the exponential function $e^{i\mathbf{g}.(\mathbf{r}_1-\mathbf{r}_2)}$ factorizes into factors of the form $e^{ig_x\pi x_1}$, each of which can be integrated separately with respect to the Cartesian coordinates of each particle, we obtain for the integral (27) (ignoring numerical factors):

$$\begin{aligned}\sum_{\mathbf{g}} v_{\mathbf{g}} &\int_0^1 e^{ig_x\pi x_1}\sin(n\pi x_1)\sin(n'\pi x_1)dx_1\\ &\times\int_0^1 e^{ig_y\pi y_1}\sin(m\pi y_1)\sin(m'\pi y_1)dy_1\\ &\times\int_0^1 e^{ig_z\pi z_1}\sin(l\pi z_1)\sin(l'\pi z_1)dz_1\\ &\times\int_0^1 e^{-ig_x\pi x_2}\sin(p\pi x_2)\sin(p'\pi x_2)dx_2\\ &\times\int_0^1 e^{-ig_y\pi y_2}\sin(q\pi y_2)\sin(q'\pi y_2)dy_2\\ &\times\int_0^1 e^{-ig_z\pi z_2}\sin(r\pi z_2)\sin(r'\pi z_2)dz_2.\end{aligned} \tag{32}$$

The one-dimensional integrals above can be performed analytically. It is convenient to define the following notation $I_k^{(0)}$ and I_{kmn} for the required elementary integrals:

$$I_k^{(0)}=\int_0^1 e^{ik\pi x}\,dx=\begin{cases}\dfrac{(-1)^k-1}{ik\pi}, & \text{if} \quad k\neq 0,\\ 1, & \text{if} \quad k=0,\end{cases}$$

and

$$I_{g_xmn}=\int_0^1 e^{ig_x\pi x}\sin(m\pi x)\sin(n\pi x)dx, \tag{33}$$

$$=\frac{1}{4}\{I^{(0)}_{n-m+g_x}+I^{(0)}_{-n+m+g_x}-I^{(0)}_{n+m+g_x}-I^{(0)}_{-n-m+g_x}\}. \tag{34}$$

The integral (32) can be conveniently expressed in terms of I as

$$\sum_{\mathbf{g}} v_{\mathbf{g}}.\{I_{g_xnn'}I_{g_ymm'}I_{g_zll'}I_{-g_xpp'}I_{-g_yqq'}I_{-g_zrr'}\}. \tag{35}$$

In this sum, enough $\mathbf{g}$-vectors need to be included to achieve convergence. The rate of convergence turns out to be largely dictated by the Coulomb singularity in the Fourier integral (30). Evidently, an evaluation in spherical polar coordinates is desirable, but the cubic boundary conditions are rather cumbersome to implement in spherical polars. On the other hand, a straightforward three-dimensional numerical Fourier transform is only slowly convergent and requires large Fourier transform meshes.

It turns out to be possible to accelerate the rate of convergence dramatically by integrating out the Coulomb singularity in a manner reminiscent of the Ewald method. To do so, we first write

$$\frac{1}{r}=\frac{\mathrm{erf}(r/\alpha)}{r}+\frac{\mathrm{erfc}(r/\alpha)}{r}, \tag{36}$$

where α is a conveniently chosen parameter. In this decomposition of $1/r$, the first term is regular at the origin:

$$\lim_{r\to 0}\frac{\mathrm{erf}(r/\alpha)}{r}=\frac{2}{\alpha\sqrt{\pi}}, \tag{37}$$

and is in fact a smooth function which can be integrated using a relatively coarse grid. The second term in (36) contains the Coulomb singularity, but is short-ranged (depending on the value of α), and the limits of integration can be extended to infinity incurring only a negligible error. The value of α needs to chosen in such a way that the integrand $\mathrm{erfc}(r/\alpha)/r$ has essentially vanished for r close to any box boundary as measured from the center. We shall see that value of the integral is remarkably insensitive to the value of α, as long as it is reasonably chosen. Taking the Fourier transform of the second term of (36) using spherical polars we obtain

$$\int\frac{e^{-i\mathbf{g}\cdot\mathbf{r}}\mathrm{erfc}(r/\alpha)}{|\mathbf{r}|}d\mathbf{r}=\frac{4\pi}{g^2}\{1-e^{-\alpha^2g^2/4}\}, \tag{38}$$

with the $g^2\to 0$ limit given by $\pi\alpha^2$.

Gathering all the expressions together, the Fourier coefficient $v_{\mathbf{g}}$ is expressed as

$$v_{\mathbf{g}}=\frac{1}{\Omega'}\int_{\Omega'}\frac{e^{-i\mathbf{g}\cdot\mathbf{r}}\,\mathrm{erf}(r/\alpha)}{|\mathbf{r}|}d\mathbf{r}+\frac{4\pi}{\Omega' g^2}\{1-e^{-\alpha^2g^2/4}\}, \tag{39}$$

and the Coulomb integral becomes

$$\begin{aligned}&(nmlpqr|n'm'l'p'q'r')\\ &\quad=\frac{2^6}{L_x}\sum_{\mathbf{g}} v_{\mathbf{g}}.\{I_{g_xnn'}I_{g_ymm'}I_{g_zll'}I_{-g_xpp'}I_{-g_yqq'}I_{-g_zrr'}\}.\end{aligned} \tag{40}$$

The convergence of the Coulomb integral as a function of the size of the Fourier transform mesh is shown in Figs. 1 and 2 for several cases of α, as well as the case for which the error function method is not used (effectively $\alpha=0$). It is clear that, without the use of the error function, the Coulomb integrals require very large FFT meshes of at least 128^3, whereas using the error function convergence is extremely rapid (requiring, conservatively, a mesh of 24^3), and fairly insensitive to the value of α.

Several features of the above method commend its use. Note that the Fourier coefficients $v_{\mathbf{g}}$, as well as the integrals I_{kmn} need to be calculated at the initialization stage once and

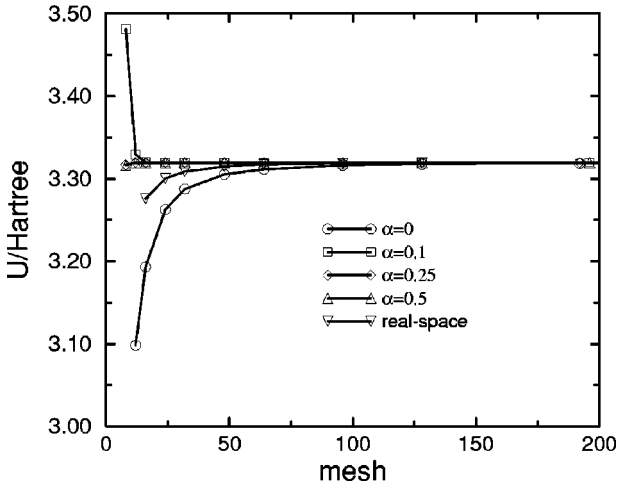

FIG. 1. Convergence of the Coulomb integral $\langle 111112^{+}|\hat{U}|111112^{+}\rangle$ as a function of the Fourier transform mesh. The real-space results are calculated according to the method outlined in the appendices. Note the fast convergence of the integral for typical values of α, as well as the insensitivity of the results to it for reasonable nonzero values of α.

for all, and stored using only a modest amount of memory. The calculation of a given Coulomb integral $(nmlpqr|n'm'l'p'q'r')$ amounts to summing over a set of tabulated values, which can be very efficiently programmed. For example, on a medium-size workstation (a 466 MHz Alpha/Compaq-ds10), nearly a million Coulomb integrals can be calculated in approximately five seconds of CPU time. For a given set of aspect ratios b and c, the Coulomb integral needs to be calculated only once for $L_x=1$. The value of a Coulomb integral for other values of L_x can be obtained simply through division by L_x, as can be seen from (40).

The above method was tested in two ways. First, by doing the Coulomb integrals using a ''brute-force'' method with a direct six-dimensional quadrature, and second using the real-space method outlined in the Appendix. The ''brute-force'' is of course extremely inefficient computationally, but has the advantage of simplicity, and helps in the weeding out of errors in the algebra, as well as programming. The

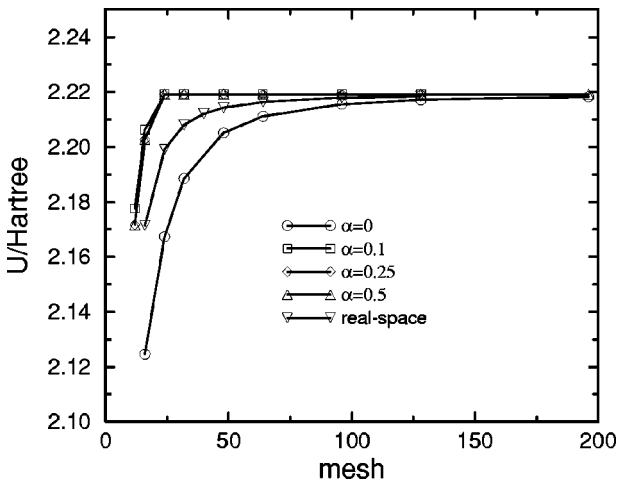

FIG. 2. The same as Fig. 1 for the symmetric state $|444443\rangle$.

TABLE I. Table of some Coulomb integrals in Hartrees, for a cubic box. A Fourier transform mesh of 32^3 was used for their evaluation.

	Symmetric	Anti-symmetric
(111111|111111)	3.0478	–
(111112|111112)	3.3198	2.1284
(111221|111221)	2.6922	2.2377
(111222|111222)	2.3606	2.1491
(111311|111311)	3.0102	2.4008
(111321|111321)	2.5940	2.3031

second method, in which the center-of-mass is integrated out, is conceptually very simple, but is rather unwieldy, as can be seen in the expressions in the Appendices. Nevertheless, it is also fairly efficient, though less so than the Fourier method, and was used as an independent cross-check of the above method. The results are plotted in Figs. 1 and 2. The methods converge asymptotically to the same result, as they should.

A sample of Coulomb integrals are given in Table I. From these we see that the Coulomb integrals between symmetric states are always larger that the anti-symmetric ones, which is simply a reflection of the fact that the anti-symmetric states tend to keep the electrons apart, and thereby lead to a smaller Coulomb interaction. The symmetric states, on the other hand, have the opposite tendency to heap the two electrons together, thereby leading to a relatively less favorable Coulomb interaction.

V. ELECTRON DENSITY AND EXCHANGE-CORRELATION HOLE

Once a two-electron wavefunction $\Psi(\mathbf{r}_1,\mathbf{r}_2)$ has been obtained as a linear expansion of two-electron basis functions $\Phi_{\mathbf{G}}$ (we omit for clarity the superscripts denoting the exact quantum numbers such as symmetry) the electron density and the physical exchange-correlation and correlation holes can be constructed. Here we shall give the expressions for future reference. The electron density $n(\mathbf{r})$ is given by the expectation value of the number density operator $\hat{n}(\mathbf{r})$:

$$\hat{n}(\mathbf{r})=\sum_i \delta(\mathbf{r}-\mathbf{r}_i), \tag{41}$$

i.e.,

$$n(\mathbf{r})=\langle\Psi|\hat{n}(\mathbf{r})|\Psi\rangle. \tag{42}$$

For the present system we obtain

$$n(\mathbf{r})=2\int |\Psi(\mathbf{r},\mathbf{r}')|^2\, d\mathbf{r}' \tag{43}$$

$$=2\sum_{\mathbf{G}\mathbf{G}'} c_{\mathbf{G}}c_{\mathbf{G}'}S_{\mathbf{G}\mathbf{G}'}(\mathbf{r}), \tag{44}$$

where the $c_{\mathbf{G}}$ are the coefficients in the wavefunction expansion (6) and

$$S_{\mathbf{G}\mathbf{G}'}(\mathbf{r})=\int d\mathbf{r}'\ \Phi_{\mathbf{G}}(\mathbf{r},\mathbf{r}')\Phi_{\mathbf{G}'}(\mathbf{r},\mathbf{r}'). \tag{45}$$

The physical exchange-correlation hole $n_{xc}(\mathbf{r},\mathbf{r}')$ is defined in terms of the expectation value of the density–density correlation function evaluated using $\Psi(\mathbf{r}_1,\mathbf{r}_2)$:

$$n_{xc}(\mathbf{r},\mathbf{r}')=(1/n(\mathbf{r}))\langle\Psi|\,\delta\hat{n}(\mathbf{r})\,\delta\hat{n}(\mathbf{r}')|\Psi\rangle-\delta(\mathbf{r}-\mathbf{r}'), \quad (46)$$

where $\delta\hat{n}(\mathbf{r})=\hat{n}(\mathbf{r})-n(\mathbf{r})$. For the present two-electron system, a numerically convenient expression for $n_{xc}(\mathbf{r},\mathbf{r}')$ can be obtained directly in terms of the wavefunction and density:

$$n_{xc}(\mathbf{r},\mathbf{r}')=\frac{2|\Psi(\mathbf{r},\mathbf{r}')|^2}{n(\mathbf{r})}-n(\mathbf{r}'), \quad (47)$$

from which the normalization of the exchange-correlation hole is immediately apparent:

$$\int n_{xc}(\mathbf{r},\mathbf{r}')d\mathbf{r}'=-1. \quad (48)$$

The correlation hole density $n_c(\mathbf{r},\mathbf{r}')$ can be computed from $n_{xc}(\mathbf{r},\mathbf{r}')$ by subtracting off the exchange-hole density $n_x(\mathbf{r},\mathbf{r}')$, which for a two-electron system is just

$$n_x(\mathbf{r},\mathbf{r}')=-n(\mathbf{r}')/2. \quad (49)$$

Thus,

$$n_c(\mathbf{r},\mathbf{r}')=\frac{2|\Psi(\mathbf{r},\mathbf{r}')|^2}{n(\mathbf{r})}-\frac{n(\mathbf{r}')}{2}. \quad (50)$$

Clearly the correlation hole is normalized to zero. The above expression (50) has a useful qualitative interpretation: $|\Psi(\mathbf{r},\mathbf{r}')|^2$ is the probability of finding one electron at position $\mathbf{r}$ and another at position $\mathbf{r}'$. Dividing this by the probability of finding an electron at $\mathbf{r}$, i.e., dividing by $n(\mathbf{r})/2$, gives the conditional probability of finding an electron at $\mathbf{r}'$ given the other one is at $\mathbf{r}$. If this conditional probability is larger than the probability of finding an electron at $\mathbf{r}'$, then $n_c(\mathbf{r},\mathbf{r}')$ is positive, and if it is less, then it is negative. When are these two situations likely to arise? Suppose $\mathbf{r}'$ is chosen to be close to the reference point $\mathbf{r}$. Then, the chances of finding another electron at $\mathbf{r}'$ given there is a different one already at $\mathbf{r}$, is likely to be small, and therefore in the vicinity of $\mathbf{r}$, the correlation hole density $n_c(\mathbf{r},\mathbf{r}')$ will be *negative*. On the other hand, if $\mathbf{r}'$ is chosen to be a large distance away from $\mathbf{r}$, then the probability of finding another electron at $\mathbf{r}'$ may be larger than average (due to correlation), and therefore $n_c(\mathbf{r},\mathbf{r}')$ may be *positive*. Electron correlation is responsible for the positive regions of the exchange-correlation hole. Therefore, by examining the oscillations in $n_c(\mathbf{r},\mathbf{r}')$ we can obtain a qualitative understanding of the spatial correlation between the two electrons in any given state Ψ. For example, if there is a physical separation of the two electrons into distinct, localized, regions of space (as it occurs in the Wigner crystal for example), then the correlation hole, and the exchange-correlation hole, will be strongly positive at separations characteristic of the lattice constant of the crystal. On the other hand if the electrons are each largely delocalized throughout all of the available space, the correlation hole will not be strongly positive, and the exchange-correlation hole density will be predominantly negative.

TABLE II. The ground state energies as a function of L and n_{max} for a tetragonal box ($b=1$, $c=1.05$). The state has ggg symmetry and $S=0$.

L/a.u.	r_s/a.u.	n_{max}	N_{basis}	E/a.u.	Relative error
10	5.00	3	76	0.5382323	0.13%
		4	288	0.5377711	0.04%
		5	1161	0.5376166	0.01%
		6	3024	0.5375660	0.005%
		7	7984	0.5375406	
50	25.0	3		0.0495036	0.6%
		4		0.0492487	0.1%
		5		0.0491938	0.01%
		6		0.0491922	0.003%
		7		0.0491908	
100	50.0	3		0.0194941	1.7%
		4		0.0192253	0.30%
		5		0.0191743	0.03%
		6		0.0191696	0.007%
		7		0.0191682	

We end by noting that the exchange-correlation hole density $n_{xc}(\mathbf{r},\mathbf{r}')$ calculated above is *not* appropriate for calculating the Kohn–Sham exchange-correlation energy $E_{xc}[n]$, which instead requires the coupling-constant-averaged exchange-correlation hole.[6] The latter will be reported in a future publication.

VI. RESULTS

We consider here a tetragonal box, in which one side is 5% longer than the other two, i.e., $b=1$, $c=1.05$. This distortion is introduced to remove a three-fold degeneracy of the $S=1$ manifold that exists at all densities in the strictly cubic box, and in addition to identify a unique reference axis. For a given n_{max}, the Hamiltonian was diagonalized using a direct diagonalization method.[11] The singlet and triplet wavefunctions of all eight symmetries (*ggg,ggu,..*, etc.) were computed. Since a direct diagonalization method was used, the calculation of the excited states within each manifold could be done with virtually no extra computational cost. This feature allowed us to investigate changes in the degeneracy of the ground and low-lying states as a function of varying density.

It is worth mentioning that the calculations do not require vast amounts of computing, and a typical complete calculation of the Coulomb integrals, the two-electron wavefunctions of the ground and excited states, together with the calculation of the density and exchange-correlation hole takes no more than a few minutes on a small workstation. As a result a large number of r_s values could be studied. In addition, it indicates that extension to a larger number of electrons, perhaps up to seven or eight electrons, is feasible using state-of-the-art machines.

A. Convergence with n_{max}

We first examine how the total energy of the system converges with increasing n_{max}, as function of $r_s=(3\Omega/8\pi)^{1/3}$. We considered values of n_{max} from 3 to 7. Table II gives the total energies for a number of r_s for the $S=0,ggg$ wavefunction, together with the number of basis functions. The energy decreases with increasing n_{max}, since

TABLE III. Ground and excited state energies (in a.u.) of the lowest two eigenstates within several manifolds. Results are obtained with $n_{\max}=5$.

$S=0$, ggg	$S=1$, ggu	$S=1$, $gug+ugg$	$S=0$, ggu	$S=0$, $ugu+guu$
$L=10$, ($r_s=5.00$)				
0.5376166	0.6156424	0.6328357	0.6944830	0.7345794
0.7610491	0.8864723	0.8784076	0.9284100	0.8688437
$L=50$, ($r_s=25.0$)				
0.0491938	0.0503273	0.0512285	0.0529397	0.0574160
0.0561794	0.0587713	0.0588106	0.0644987	0.0624781

of course it is variational with respect to it. The relative error is defined with respect to the energy using $n_{\max}=7$. It can be seen that increasing r_s gives rise to slightly slower convergence, as measured by the relative error. Despite this, however, it can be seen that extremely accurate energies can be obtained, with relative errors of 0.01% using $n_{\max}=5$, corresponding to approximately 1000 basis functions, and more accurate energies can be obtained with rather modest computational requirements up to about $n_{\max}=7$.

We give in Table III a set of low-lying excited state energies within several manifolds, which may be of future use as benchmark data.

B. Energies vs r_s

The lowest energy singlet and triplet states, as well as a number of excited states, were computed from $r_s=0.5$ to 50 in intervals of 0.5 a.u. At small r_s, the leading term in the energy is dominated by the kinetic energy, and therefore the energy goes as $E\sim A/r_s^2+B/r_s+\cdots$, where A and B are constants. We have therefore scaled the energies by r_s^2, so that they tend, in the limit of $r_s\to 0$ to a constant, as shown in Fig. 3.

The ground state is a $S=0$ singlet function with ggg symmetry at all r_s. As a function of r_s, the singlet ground state energy appears to change smoothly. By contrast, the

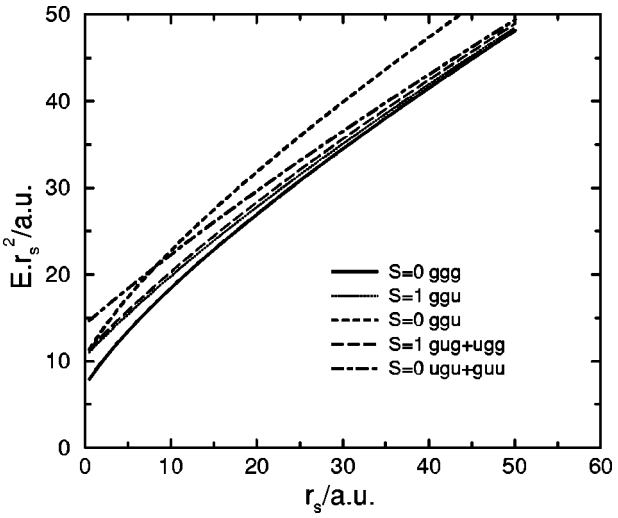

FIG. 3. The energies of the ground state and low-lying excited states vs r_s for the tetragonally distorted box ($b=1$, $c=1.05$). The overall ground state is $S=0,ggg$. Note the crossing of the $S=0,ggu$ and ugu at $r_s\approx 8$. For clarity, the energies of the triplet state are shown with the thin lines.

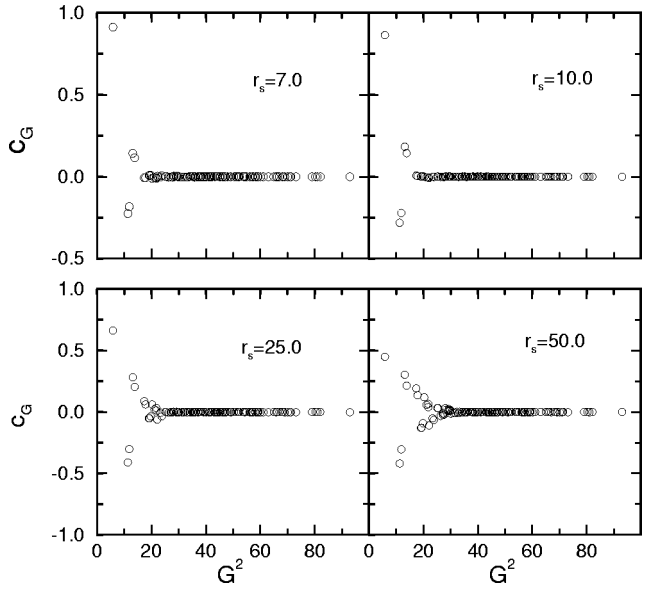

FIG. 4. Wavefunction coefficients for the $S=0,ggg$ ground state at several r_s, obtained with $n_{\max}=4$.

first-excited state of the singlet manifold exhibits a nonanalytic change of slope at $r_s\approx 8$. This due is to a crossing of states with different symmetry. For r_s smaller than this value, the first-excited state of the $S=0$ manifold has ggu symmetry. It is therefore nondegenerate, (remembering that the tetragonal distortion is along the z-axis). At the crossover point, the states with ugg and gug, which are a degenerate pair in the tetragonal box, drop below the ggu manifold. Thus the first excited state changes its symmetry, and degeneracy, at this cross over. As we shall see below, this change signals the onset of a qualitative change in the appearance of the ground state density. To summarize, therefore, the ordering of the levels of the $S=0$ manifold is

$$E_{ggg}<E_{ggu}<E_{gug}=E_{ugu}\ldots, \quad \text{for } r_s<8, \tag{51}$$

$$E_{ggg}<E_{gug}=E_{ugu}<E_{ggu}\ldots, \quad \text{for } r_s>8. \tag{52}$$

The lowest energy state of the triplet ($S=1$) manifold has ggu symmetry at all r_s. At all r_s studied, the first excited state of is the degenerate pair gug and ugg. However the ordering of the remaining states changes several times as r_s is increased and the behavior seems rather subtle. However, we can say that the global ordering of the states, taking all the quantum numbers into account, is

$$E_{ggg}^{S=0}<E_{ggu}^{S=1}<E_{gug}^{S=1}=E_{ugg}^{S=1}<E_{ugu}^{S=0}\ldots, \quad \text{for } r_s<8, \tag{53}$$

$$E_{ggg}^{S=0}<E_{ggu}^{S=1}<E_{gug}^{S=1}=E_{ugg}^{S=1}<E_{gug}^{S=0} =E_{ugu}^{S=0}\ldots, \quad \text{for } r_s>8. \tag{54}$$

C. The ground state wavefunction

It is of some interest to see how the wavefunctions evolve as a function of r_s. We concentrate here on the overall ground state ($S=0$, ggg). The wavefunction coefficients are shown in Figs. 4. As r_s increases, there is a smooth decrease in the contribution of the $|111111\rangle$ basis function, together with an increase in the contributions from higher

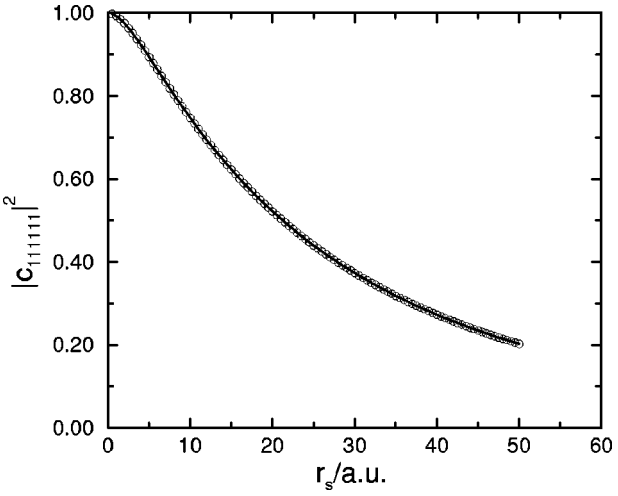

FIG. 5. The square-amplitude of the coefficient of the lowest kinetic-energy basis function ($|111111\rangle$) for the ground state, as a function of r_s.

ggg basis functions such as $|111113\rangle$,$|111131\rangle$, $|111311\rangle$,$|112112\rangle$,$|121121\rangle$,$|211211\rangle$. In Fig. 5 we show the contribution of the lowest kinetic-energy basis function ($|111111\rangle$) to the ground state wavefunction as r_s increases. At small r_s, the behavior of $|c_{111111}|^2$ as a function of r_s can be fit quite well by a stretched exponential of the form $e^{-\beta r_s^{\alpha}}$ with noninteger α, whereas at higher r_s the behavior is better fit by a simple form $e^{-(a_0+a_1 r_s+a_2 r_s^2)}$.

D. The ground state density

The density of the singlet ground state is shown in Fig. 6 as an isodensity plot for several values of r_s, together with the expectation value of the density along the z and x axes, i.e., $\langle n(z)\rangle$ and $\langle n(x)\rangle$, in Figs. 7 and 8. At high densities ($r_s<7$), the electron density has a maximum in the box center with respect to all three Cartesian axes. At $r_s\approx 7$, the density acquires a minimum along the z-axis at the box center, while remaining a maximum there along the x- and y-axes. At $r_s\approx 8$, the density acquires a minimum along the x- and y-axes at the center of the box. The asymmetry which appears here between the behavior of the electron density in the z and x,y directions is, of course, due to the tetragonal distortion we have introduced; in a cubic box, these minima (by symmetry) would all appear at the same value of r_s. Subsequent lowering of the density gives rise successively to a deeper minimum at the box center, and the simultaneous localization of the electrons into the eight corners of the box. This latter state can be viewed as the ''Wigner'' crystal limit of the present model. Thus the density of $r_s\approx 8$ can be identified as the onset of the ''Wigner'' crystal. The state can be associated with the density acquiring a minimum not only with respect to the long axis of the box, but also with respect to the two short axes.

As noted earlier, at the same $r_s\approx 8$, there is a crossover of states, changing the first excited state from ggu to gug symmetry.

Accompanying the transition to the ''Wigner'' crystal are noticeable changes in the correlation hole density $n_c(\mathbf{r},\mathbf{r}')$ computed from Eq. (50). Since this is a six-dimensional function, visualizing it is difficult. The main correlation effect is along the (111) body diagonal; therefore we show in Fig. 9 $n_c(\mathbf{r},\mathbf{r}')$ along the (111) body diagonal, i.e., we let

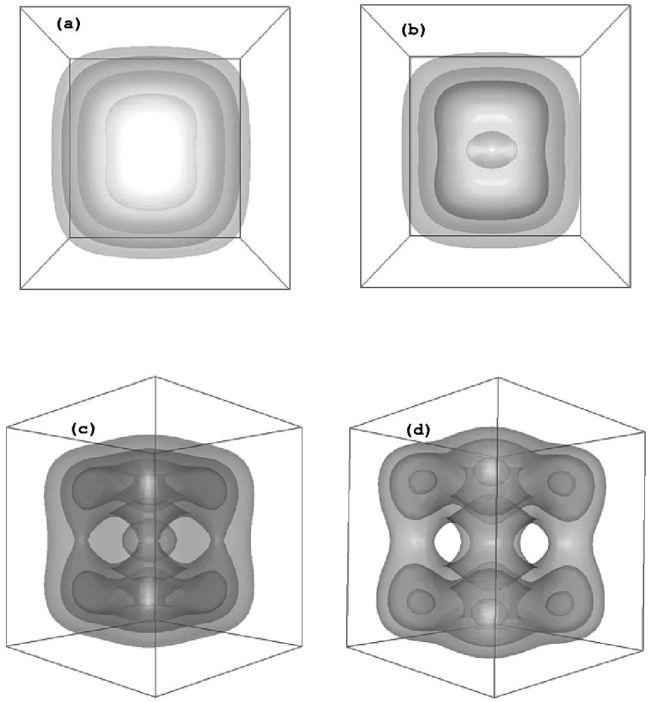

FIG. 6. Singlet ($S=0,ggg$) electron density maps at (a) $r_s=7.0$, (b) $r_s=10.0$, (c) $r_s=25.0$, (d) $r_s=50.0$ for the tetragonally distorted box $b=1$, $c=1.05$. The view in (c) and (d) has been rotated around the z-axis to show the accumulation of electron density in the box corners as the density is lowered.

$$\mathbf{r}'=\mathbf{r}+\lambda(1\hat{1}1)^T, \tag{55}$$

choosing two reference points for $\mathbf{r}$, i.e., $\mathbf{r}=\mathbf{r}_b$ and $\mathbf{r}=\mathbf{r}_c$ with

$$\mathbf{r}_b=(L_x/2,L_y/2,L_z/2)^T, \quad \mathbf{r}_c=(L_x/16,L_y/16,L_z/16)^T, \tag{56}$$

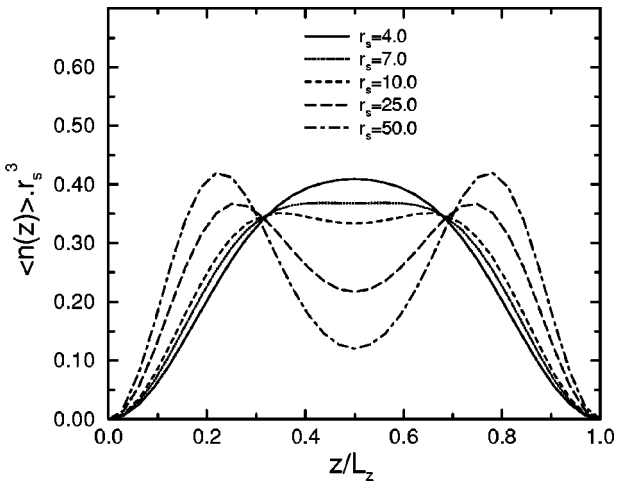

FIG. 7. $\langle n(z)\rangle$ for the ground state at several densities. Note that a minimum appears in $\langle n(z)\rangle$ at the midway point for $r_s\approx 7.0$.

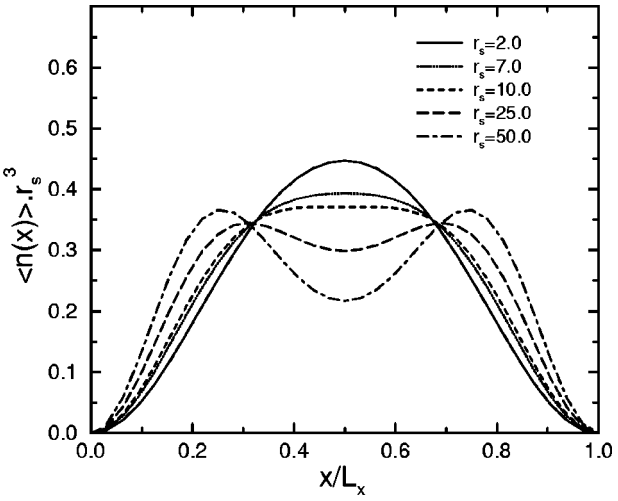

FIG. 8. $\langle n(x)\rangle$ for the ground state at several densities. A minimum in the box center is visible for $r_s=10$, but not at $r_s=7$.

i.e., box center and a box corner, respectively. In Eq. (55) λ is a scalar which measures the distance of $\mathbf{r}'$ from $\mathbf{r}$. Let us consider the observed behavior. Suppose we first fix our attention at the box center, i.e., let $\mathbf{r}=\mathbf{r}_b$. For small r_s, the density $n(\mathbf{r})$ is a maximum there, and correspondingly the $n_c(\mathbf{r}_b,\mathbf{r}')$ has a deep minimum, and, of course, a negative value. As we move $\mathbf{r}'$ along the (111) body diagonal, the density $n(\mathbf{r}')$ drops, and, correspondingly, $n_c(\mathbf{r}_b,\mathbf{r}')$ steadily increases towards zero, becoming slightly positive, before attaining zero upon reaching either box corner. At high r_s, however, the behavior is quite different. In this case, the box center is in fact a minimum in density, and, correspondingly, although $n_c(\mathbf{r}_b,\mathbf{r}_b)$ is negative, actually corresponds to a local maximum along the (111) direction. As we move $\mathbf{r}'$ along the (111) direction, the electron density increases (as the electrons are localizing in the box corners), and, correspondingly, $n_c(\mathbf{r}_b,\mathbf{r}')$ splits into two symmetric

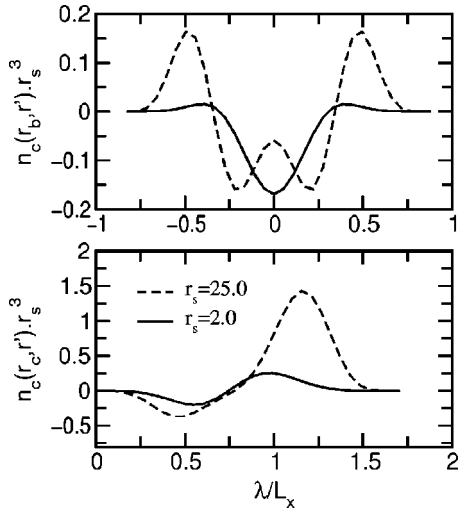

FIG. 9. Correlation hole density $n_c(\mathbf{r},\mathbf{r}').r_s^3$ for two values of r_s for the singlet ground state. Two reference points $\mathbf{r}$ are shown (a) $\mathbf{r}=\mathbf{r}_b$; (b) $\mathbf{r}=\mathbf{r}_c$. The points $\mathbf{r}'$ are chosen according to Eq. (55). On the graphs, the point $\lambda=0$ corresponds to $\mathbf{r}'=\mathbf{r}$, i.e., the position of the point $\mathbf{r}'$ coinciding with that of the reference point $\mathbf{r}$.

minima. As we move $\mathbf{r}'$ towards either box corner, $n_c(\mathbf{r}_b,\mathbf{r}')$ becomes strongly positive, indicating a strongly enhanced probability of finding the other electron in a box corner.

Consider now the reference point $\mathbf{r}$ close to a box corner (i.e., $\mathbf{r}=\mathbf{r}_c$). At low r_s, the density $n(\mathbf{r})$ there is very low. Therefore the correlation hole starts off close to zero, and as we move $\mathbf{r}'$ along the body diagonal, it gradually becomes negative, acquiring a shallow minimum in that direction, followed by a shallow positive maximum. At high r_s, as $\mathbf{r}'$ is moved along the (111) body diagonal, the correlation hole first of all acquires a minimum, and then upon moving farther away from $\mathbf{r}_c$ along the body diagonal, becomes strongly positive and acquires a maximum. The strong maximum in the correlation hole is arising because the electrons are localized into the box corners, since if we specify one electron to be in the box corner $\mathbf{r}_c$, this greatly enhances the probability of finding the *other* electron in the diagonally opposite box corner.

Of course the analogy with ''Wigner''-crystallization should not be stretched. In the present system, it is not possible for each electron to become strictly localized in a corner, as there are only two electrons and eight corners. However, in the low-density limit, the most likely place to find an electron is in a corner, and, furthermore, if one electron is at one corner, the other electron is in the opposite corner. What exists in this limit is the strong *correlation* across the body diagonal of the box.

VII. CONCLUSION

In this paper we have studied the quantum-mechanical behavior of two electrons confined to a box with hard walls in an essentially exact way. An exact diagonalization method is used, in which the wavefunctions are expressed as a linear combination of symmetrized or anti-symmetrized trigonometric functions, which can be further classified according to their symmetry under reflection operations of the cube. The Coulomb integrals are shown to be amenable to an efficient and accurate calculation. A study of the convergence of the total energy with respect to the maximum wavenumber shows that down to densities of $r_s=50$, highly accurate energies can be obtained using $n_{\max}=5$. A strength of the present approach is that it does not make assumptions regarding the nodal structure of the ground (or excited) state wavefunctions.

Using this method we studied the behavior of the ground and first few excited states of the system as a function of increasing r_s. The ground state is an $S=0$, ggg function at all densities. A ''Wigner'' crystal arises as r_s is increased, and the onset of this is associated with the change in symmetry of the first excited state of the $S=0$ manifold.

The present model presents us with a new type of essentially exactly solvable electronic system. Due to the absence of a centrally attractive potential, the observed correlation is between free, yet confined, electrons. The computational effort required to solve the present two electron system is extremely modest, with physical results being obtained with the diagonalization of matrices of the order of several hundred.

The present approach is being extended to a greater number of electrons. It may be an ideal model to study a number of issues of extraordinary interest, such as electron correlation in ground and excited state density functionals. In addition, since excited states can be calculated, studying time-dependent problems, and systems in magnetic fields, as well as modeling of quantum dots, is feasible within the current framework.

ACKNOWLEDGMENTS

It is a pleasure to acknowledge stimulating discussions with Professor R. M. Lynden-Bell, Professor M. W. Finnis, Dr. J. Kohanoff, and Dr. T. Todorov.

APPENDIX A: REAL-SPACE EVALUATION OF THE COULOMB INTEGRALS

We give for interested readers the derivation of the Coulomb integrals using a real-space method and a transformation of variables. Let

$$x = x_1 - x_2, \tag{A1}$$

$$X = x_1 + x_2, \tag{A2}$$

with similar definitions for y,Y and z,Z. The Jacobian for this transformation is

$$J(x,X,x_1,x_2) = 1/2. \tag{A3}$$

The limits of integration are changed as follows:

$$\int_{x_1=0}^{1}\int_{x_2=0}^{1} dx_1\, dx_2 \rightarrow \frac{1}{2}\left(\int_{x=0}^{1}\int_{X=x}^{2-x} dX\, dx + \int_{x=-1}^{0}\int_{X=-x}^{x-2} dX\, dx \right). \tag{A4}$$

The Coulomb integral (27) can be transformed using the coordinates x,y,z and X,Y,Z, followed by integration over X,Y,Z. This can be affected in an elementary though tedious way. Consider first the factors numerator in the Coulomb integral (23) which involve the coordinates x_1 and x_2:

$$\begin{aligned}&\sin(n\pi x_1)\sin(p\pi x_2)\sin(n'\pi x_1)\sin(p'\pi x_2)\\ &= \sin\left(n\pi\frac{X+x}{2}\right)\sin\left(p\pi\frac{X-x}{2}\right)\sin\left(n'\pi\frac{X+x}{2}\right)\\ &\quad\times\sin\left(p'\pi\frac{X-x}{2}\right).\end{aligned} \tag{A5}$$

Next we integrate out X from $X=x$ to $X=2-x$, leaving only a function of x. It is convenient to introduce the following function of x:

$$\begin{aligned}G_{npn'p'}(x) = \int_x^{2-x} dX \sin\left(n\pi\frac{X+x}{2}\right)\sin\left(p\pi\frac{X-x}{2}\right)\\ \times\sin\left(n'\pi\frac{X+x}{2}\right)\sin\left(p'\pi\frac{X-x}{2}\right).\end{aligned} \tag{A6}$$

A similar function could be defined to handle the second integral over X (from $X=-x$ to $X=x-2$) that appears in (A4), but this can be expressed in terms of $G_{pnp'n'}(-x)$. Thus the two integrals in (A4) over X appear in the pair:

$$\frac{1}{2}\{G_{npn'p'}(x) + G_{pnp'n'}(-x)\}.$$

Analytic expressions for G will be provided in Appendix B. The Coulomb integral can be expressed as a product of three functions involving G, multiplied by $1/r$. Thus:

$$\begin{aligned}&(nmlpqr|n'm'l'p'q'r')\\ &= \frac{2^3}{L_x}\int_0^1\int_0^1\int_0^1 \{G_{npn'p'}(x) + G_{pnp'n'}(-x)\}\\ &\quad\times\{G_{mqm'q'}(y) + G_{qmq'm'}(-y)\}\\ &\quad\times\frac{\{G_{lrl'r'}(z) + G_{rlr'l'}(-z)\}}{\sqrt{x^2+b^2y^2+c^2z^2}}\,dx\,dy\,dz.\end{aligned} \tag{A7}$$

This three-dimensional integral can be evaluated using a numerical grid. In Figs. 1 and 2 are plotted two examples of Coulomb integrals evaluated using this real-space method.

APPENDIX B: EVALUATION OF *G*

By application of the cosine addition formula,

$$2\sin(a)\sin(b) = \cos(a-b) - \cos(a+b),$$

to the rhs of Eq. (A5), followed by an expansion of a product of sums of cosines, we arrive at

$$\begin{aligned}G_{nmpq}(x) = \frac{1}{4}\int_x^{2-x} dX\Bigg[&\cos\left((n-p)\pi\frac{X+x}{2}\right)\\ &\times\cos\left((m-q)\pi\frac{X-x}{2}\right) - \cos\left((n-p)\pi\frac{X+x}{2}\right)\\ &\times\cos\left((m+q)\pi\frac{X-x}{2}\right) - \cos\left((n+p)\pi\frac{X+x}{2}\right)\\ &\times\cos\left((m-q)\pi\frac{X-x}{2}\right) + \cos\left((n+p)\pi\frac{X+x}{2}\right)\\ &\times\cos\left((m+q)\pi\frac{X-x}{2}\right)\Bigg].\end{aligned} \tag{B1}$$

Each of the above integrals can be done. Let us define

$$J_{kl}(x) = \int_x^{2-x} dX \cos\left(k\pi\frac{X+x}{2}\right)\cos\left(l\pi\frac{X-x}{2}\right), \tag{B2}$$

in terms of which G can be expressed as

$$\begin{aligned}G_{nmpq}(x) = \frac{1}{4}(&J_{n-p,m-q}(x) - J_{n-p,m+q}(x)\\ &- J_{n+p,m-q}(x) + J_{n+p,m+q}(x)).\end{aligned} \tag{B3}$$

There are five cases to be handled, depending on the values of k and l.

(i) $|k| \neq |l| \neq 0$:

$$J_{kl}(x)=\frac{2k\sin(k\pi x)-(k-l)\,(\pi(k+l-l\,x))-(k+l)\,(\pi(k-l+l\,x))}{(-k^2+l^2)\,\pi}. \tag{B4}$$

(ii) $|k|=|l|\neq 0$:

$$J_{kk}(x)=\cos(k\pi x)-x\cos(k\pi x)+\frac{\sin(k\pi(2-x))}{2k\pi}-\frac{\sin(k\pi x)}{2k\pi}. \tag{B5}$$

(iii) $k=0$, $l\neq 0$:

$$J_{0l}(x)=\frac{2\sin(l\pi(1-x))}{l\pi}. \tag{B6}$$

(iv) $l=0$, $k\neq 0$:

$$J_{k0}(x)=\frac{-2\sin(k\pi x)}{k\pi}. \tag{B7}$$

(iv) $k=l=0$:

$$J_{00}(x)=2-2x. \tag{B8}$$

[1] R. G. Parr and W. Yang, *Density Functional Theory of Atoms and Molecules* (Oxford University Press, New York, 1989).
[2] R. M. Driezler and E. K. U. Gross, *Density Functional Theory* (Springer-Verlag, Berlin, 1990).
[3] J. P. Perdew, K. Burke, and Y. Wang, Phys. Rev. B **54**, 16533 (1996).
[4] P. Hohenberg and W. Kohn, Phys. Rev. B **3**, 864 (1964).
[5] W. Kohn and L. Sham, Phys. Rev. A **140**, 113 (1965).
[6] O. Gunnarson and B. I. Lundqvist, Phys. Rev. B **13**, 4274 (1975).
[7] N. R. Kestner and O. Sinanoglou, Phys. Rev. **128**, 2687 (1962).
[8] P. M. Laufer and J. B. Krieger, Phys. Rev. A **33**, 1480 (1986).
[9] S. Kais, D. R. Herschbach, and R. D. Levine, J. Chem. Phys. **91**, 7791 (1989).
[10] S. Kais, D. R. Herschbach, N. C. Handy, C. W. Murray, and G. J. Laming, J. Chem. Phys. **99**, 417 (1993).
[11] We used the real-symmetric diagonalization routine DSYEVX of the LAPACK package.